

# Geophysical Research Letters<sup>®</sup>



## RESEARCH LETTER

10.1029/2021GL095680

## Stable Barium Isotope Dynamics During Estuarine Mixing

### Key Points:

- We present dissolved Ba isotopic compositions covering the entire salinity gradient in the large Yangtze and Pearl River Estuary in Asia
- Particle adsorption-desorption induces Ba isotope fractionation at low salinities and alters Ba properties of the river water endmember
- Conservative mixing dominates Ba isotope distributions at high salinities providing a calibration for using it as a paleosalinity proxy

Zhimian Cao<sup>1</sup> , Xinting Rao<sup>1</sup>, Yang Yu<sup>2</sup> , Christopher Siebert<sup>2</sup>, Ed C. Hathorne<sup>2</sup> , Bo Liu<sup>3</sup> , Guizhi Wang<sup>1</sup> , Ergang Lian<sup>4</sup> , Zhibing Wang<sup>5</sup> , Ruifeng Zhang<sup>6</sup> , Lei Gao<sup>7</sup> , Gangjian Wei<sup>5</sup> , Shouye Yang<sup>4</sup> , Minhan Dai<sup>1</sup> , and Martin Frank<sup>2</sup>

<sup>1</sup>State Key Laboratory of Marine Environmental Science and College of Ocean and Earth Sciences, Xiamen University, Xiamen, China, <sup>2</sup>GEOMAR Helmholtz Center for Ocean Research Kiel, Kiel, Germany, <sup>3</sup>Alfred Wegener Institute Helmholtz Centre for Polar and Marine Research, Bremerhaven, Germany, <sup>4</sup>State Key Laboratory of Marine Geology, Tongji University, Shanghai, China, <sup>5</sup>State Key Laboratory of Isotope Geochemistry, Guangzhou Institute of Geochemistry, Chinese Academy of Sciences, Guangzhou, China, <sup>6</sup>School of Oceanography, Shanghai Jiao Tong University, Shanghai, China, <sup>7</sup>State Key Laboratory of Estuarine and Coastal Research, East China Normal University, Shanghai, China

### Supporting Information:

Supporting Information may be found in the online version of this article.

### Correspondence to:

Z. Cao,  
[zmcao@xmu.edu.cn](mailto:zmcao@xmu.edu.cn)

### Citation:

Cao, Z., Rao, X., Yu, Y., Siebert, C., Hathorne, E. C., Liu, B., et al. (2021). Stable barium isotope dynamics during estuarine mixing. *Geophysical Research Letters*, 48, e2021GL095680. <https://doi.org/10.1029/2021GL095680>

Received 11 AUG 2021  
Accepted 8 SEP 2021

**Abstract** Stable barium isotopes are a potential proxy for riverine inputs into the ocean that reflect monsoon variability and climate change. However, dissolved Ba isotope ( $\delta^{138}\text{Ba}_{\text{DBa}}$ ) geochemistry in river estuaries, a dynamic land to ocean transition zone, has rarely been systematically examined to date. Here, we show that significant Ba isotope fractionation occurs at near-zero salinities in the Yangtze and Pearl River Estuary, whereas conservative mixing dominates  $\delta^{138}\text{Ba}_{\text{DBa}}$  distributions beyond low salinities, which are well predicted by an ion exchange model. Elevated  $\delta^{138}\text{Ba}_{\text{DBa}}$  in the river endmember results from preferential removal of light Ba isotopes by adsorption to fluvial particles. Subsequently,  $\delta^{138}\text{Ba}_{\text{DBa}}$  rapidly drops to minimum signatures at increased salinities indicating particle desorption of isotopically light Ba. Nevertheless, the apparently conservative  $\delta^{138}\text{Ba}_{\text{DBa}}$ -salinity relationship beyond the low-salinity minimum in both estuaries provides a modern calibration for using Ba isotopes as a proxy for paleosalinity and river water inputs into the ocean.

**Plain Language Summary** Barium is a nutrient-type trace element in the ocean and has been widely used for tracing circulation, biological productivity, and land-ocean interactions. Riverine input is the largest source of oceanic Ba but the Ba properties of this input can be altered during transport along river estuaries. The recent development of stable Ba isotope measurements provides a novel tool to investigate the geochemical behavior of Ba during estuarine mixing between river water and seawater. We thus systematically investigated the dissolved Ba isotope distributions along the entire salinity gradient in two Asian large river estuaries. We found that significant Ba isotope fractionation occurs at near-zero salinities in the Yangtze and Pearl River Estuary, which mainly results from particle adsorption-desorption processes. This fractionation substantially alters the original Ba properties of the river water endmember and significantly affects the global ocean Ba mass balance. Beyond low salinities of both estuaries, however, Ba isotopes and salinity show a conservative relationship predominantly controlled by water mass mixing. This is an important calibration for using stable Ba isotopes as a proxy for past sea surface salinity under the influence of large river plumes, which reflects the variability of precipitation and the impact of climate change.

## 1. Introduction

Accurate reconstruction of changes in precipitation on the continents via sea surface salinity in the adjacent ocean is of great importance to understand the monsoon system and assess the impacts of climate change. The barium to calcium (Ba/Ca) ratio recorded by marine calcifiers such as planktonic foraminifera and corals is widely used as a quantitative proxy for paleosalinity in the proximity to large river plumes significantly enriched in Ba at low salinities, and has been linked to climate-driven changes in monsoon intensity and land-sea interactions (Gebregiorgis et al., 2016; Lewis et al., 2018; Tanzil et al., 2019; Weldeab et al., 2007, 2011, 2014). Because Ca, a major element in carbonate archives, is normally conservative in estuaries, this approach is mainly based on the unique behavior of Ba during estuarine mixing.

© 2021. The Authors.

This is an open access article under the terms of the [Creative Commons Attribution-NonCommercial-NoDerivs License](https://creativecommons.org/licenses/by-nc-nd/4.0/), which permits use and distribution in any medium, provided the original work is properly cited, the use is non-commercial and no modifications or adaptations are made.

Generally, dissolved barium concentrations (DBa) in estuaries show a consistent two-stage distribution pattern: a marked increase is observed between zero salinity ( $DBa_{sal=0}$ ) and a concentration maximum ( $DBa_{max}$ ) at low salinities of 5–10, followed by a linear decrease with increasing salinity toward 33–35 in coastal environments (Edmond et al., 1985; Guay & Falkner, 1998; Joung & Shiller, 2014). Extrapolation of the latter to zero salinity defines the effective river water endmember concentration ( $DBa_{eff}$ ; Coffey et al., 1997), which is significantly higher than  $DBa_{sal=0}$  and generally ascribed to adsorption of Ba to suspended fluvial particles (Hanor & Chan, 1977; Samanta & Dalai, 2016). Subsequent salinity-induced desorption controls the  $DBa_{max}$  signatures but their peak values and corresponding salinity vary among estuaries (Coffey et al., 1997; Guay & Falkner, 1998; Joung & Shiller, 2014).

Beyond  $DBa_{max}$ , the clear negative DBa-salinity linear relationship suggests that conservative mixing dominates surface DBa concentrations that have thus been applied to trace present and past riverine inputs into the ocean (Gebregiorgis et al., 2016; Guay & Falkner, 1997; Lewis et al., 2018; Samanta & Dalai, 2016; Tanzil et al., 2019; Weldeab et al., 2007, 2011, 2014). The exact mechanisms controlling DBa dynamics and  $DBa_{max}$  during estuarine mixing are, however, not fully constrained (Colbert & McManus, 2005; Hong et al., 2018; Moore, 1997). Moreover, the reliability of the Ba/Ca ratio as a tracer of past freshwater discharge is still under debate because deviations from the conservative DBa-salinity relationship and seasonal variability of the linear regression pattern at high salinities have been observed in some estuaries (Joung & Shiller, 2014; Stecher & Kogut, 1999).

Inspired by the pioneering study of von Allmen et al. (2010), recent measurements of stable Ba isotopic compositions of seawater and river waters ( $\delta^{138}Ba_{DBa}$ ; Bates et al., 2017; Bridgestock et al., 2018, 2021; Cao, Li, et al., 2020; Cao, Siebert, et al., 2020; Geyman et al., 2019; Gou et al., 2020; Hemsing et al., 2018; Horner et al., 2015; Hsieh & Henderson, 2017; Pretet et al., 2016) have provided a new avenue to better understand the biogeochemistry of Ba in river estuaries. These studies have shown that major rivers are generally characterized by relatively light  $\delta^{138}Ba_{DBa}$  signatures (0.2‰–0.3‰ on average), reflecting dissolution of lithogenic material, whereas surface seawater shows significantly heavier  $\delta^{138}Ba_{DBa}$  signatures (around 0.6‰) due to preferential removal of light Ba isotopes from the dissolved phase via adsorption to or incorporation into particulate phases. However, to date there are few complete views of Ba isotope distributions along the entire salinity gradient in estuaries. To elucidate the geochemical processes controlling Ba isotopes during estuarine mixing and their potential as a new proxy for precipitation on land, we systematically examine the factors controlling surface  $\delta^{138}Ba_{DBa}$  in two of the world's largest river estuaries, the Yangtze and Pearl River Estuary (YRE and PRE, respectively; Figure 1; Table S1) during different seasons. To support our data interpretation, an ion-exchange model is applied to simulate  $\delta^{138}Ba_{DBa}$  distributions and constrain Ba isotope fractionation during particle adsorption-desorption in estuarine environments.

Our findings show that measured  $\delta^{138}Ba_{DBa}$  signatures at zero salinity in both estuaries are elevated, mainly as a result of preferential adsorption of light Ba isotopes to fluvial particles. At slightly increased salinities corresponding to  $DBa_{max}$  concentrations, we infer that desorption of isotopically light Ba from suspended particles induces a “drop” of  $\delta^{138}Ba_{DBa}$ . Toward the open ocean endmember, conservative two-endmember mixing between low-salinity waters at  $DBa_{max}$  and seawater can fully explain the  $\delta^{138}Ba_{DBa}$ -salinity relationship. Our results improve the understanding of Ba isotope geochemistry in river estuaries and of the connection between the oceanic and terrestrial Ba cycles, which is crucial for the quantification of present and past riverine inputs and the current Ba mass balance in the ocean.

## 2. Methods

### 2.1. Ba Isotope Analyses

Ba isotopic compositions ( $\delta^{138}Ba = [(^{138}Ba/^{134}Ba)_{sample}/(^{138}Ba/^{134}Ba)_{standard} - 1] \times 1000$ , in ‰) were measured at Xiamen University following the method in Cao, Siebert, et al. (2020), which consists of double spiking, ion-exchange chromatography, and analysis by MC-ICP-MS. The external reproducibility for the replicate measurements of an in-house seawater matrix standard was  $\pm 0.05\%$  (2SD,  $N = 13$ ). Our  $\delta^{138}Ba$  measurements of the GEOTRACES SAFe seawater reference material (surface:  $+0.62 \pm 0.04\%$ , 2SD,  $N = 2$  and deep:  $+0.28 \pm 0.09\%$ , 2SD,  $N = 2$ ) are within error identical to those reported by three other labs (Geyman

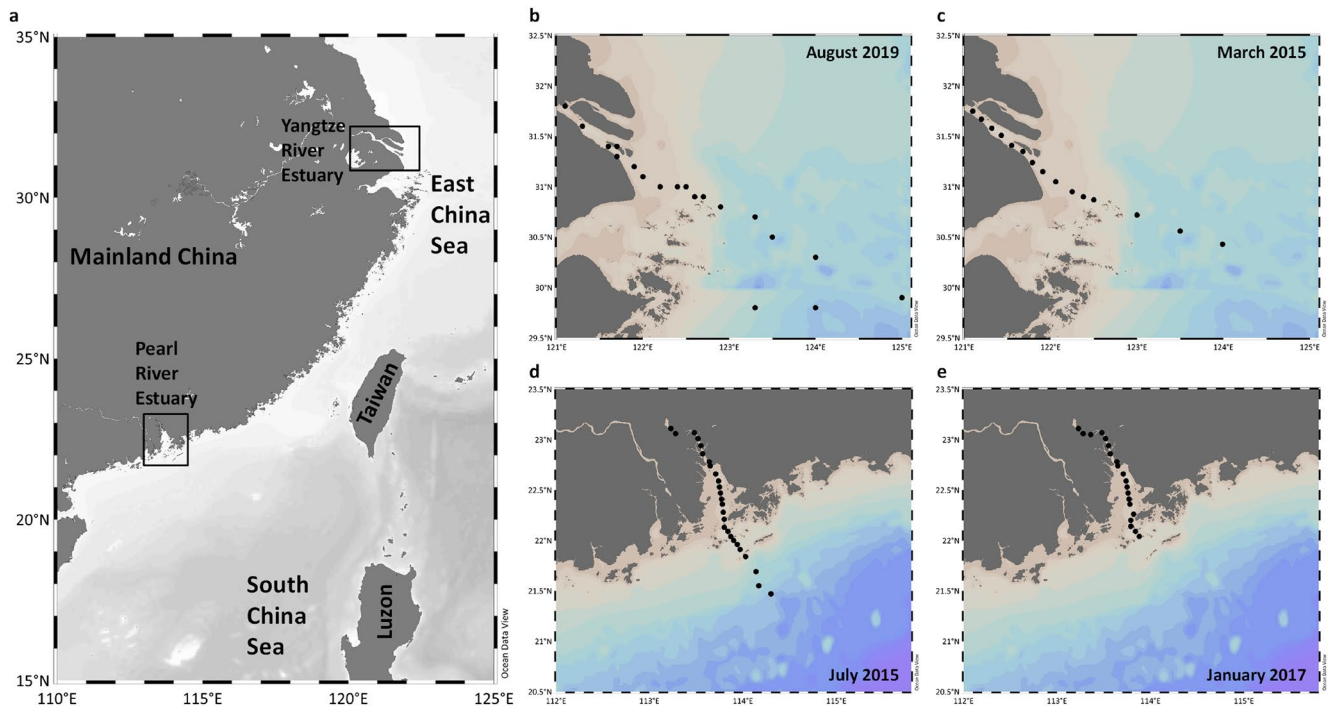


**Figure 1.** Sampling sites in the Yangtze and Pearl River Estuary and adjacent shelf areas. (a) Location of the two estuaries; (b and c) Stations in the Yangtze River Estuary and East China Sea shelf in August 2019 and March 2015, respectively; (d and e) Stations in the Pearl River Estuary and South China Sea shelf in July 2015 and January 2017, respectively. Maps were created with ODV (Schlitzer, 2021).

et al., 2019; Hsieh & Henderson, 2017; Yu et al., 2020). Details of the Ba isotope analyses are provided in the Supporting Information S1.

## 2.2. Ion Exchange Model

During estuarine mixing Ba adsorbed to suspended fluvial particles is replaced by dissolved major cations including Mg and Ca due to similar physicochemical properties of alkaline(-earth) metals. Ion exchange expressions were thus used to develop a predictive model as shown in Hanor and Chan (1977). We extended this model to predict surface  $\delta^{138}\text{Ba}_{\text{DBa}}$  distributions in estuaries by simultaneously calculating dissolved  $^{138}\text{Ba}$  and  $^{134}\text{Ba}$  concentrations. Various concentrations and isotopic compositions of exchangeable Ba on suspended fluvial particles were tested and assigned in the model. Details of the ion exchange model are provided in the Supporting Information S1.

## 3. Results and Discussion

### 3.1. Surface DBa Distributions

Our new DBa concentration data confirm the distribution pattern generally observed in large river estuaries (Edmond et al., 1985; Guay & Falkner, 1998; Joung & Shiller, 2014). In the YRE, surface DBa and salinity show a significant negative linear relationship at salinities  $>4.6$  in summer (August 2019;  $R^2 = 0.97$ ,  $P < 0.0001$ ,  $N = 16$ ) and  $>7.5$  in spring (March 2015;  $R^2 = 0.97$ ,  $P < 0.0001$ ,  $N = 7$ ), demonstrating conservative estuarine mixing beyond low salinities. The  $\text{DBa}_{\text{max}}$  is distinct around  $490 \text{ nmol kg}^{-1}$  in summer but could not be defined in spring, likely due to poor sampling resolution. By extrapolating the DBa-salinity linear regressions to zero salinity,  $\text{DBa}_{\text{eff}}$  concentrations of 565 and  $450 \text{ nmol kg}^{-1}$  are obtained, which are markedly higher than the corresponding  $\text{DBa}_{\text{sal}=0}$ , particularly in the former case (Figures 2a and 2c). A  $\text{DBa}_{\text{eff}}$  of  $525 \text{ nmol kg}^{-1}$  at zero salinity and a  $\text{DBa}_{\text{max}}$  of  $370 \text{ nmol kg}^{-1}$  at a salinity of 12 were previously reported for the YRE in summer (June 1980), during which a broad DBa plateau was observed from the river endmember to the location of the  $\text{DBa}_{\text{max}}$  (Figure S1; Edmond et al., 1985).

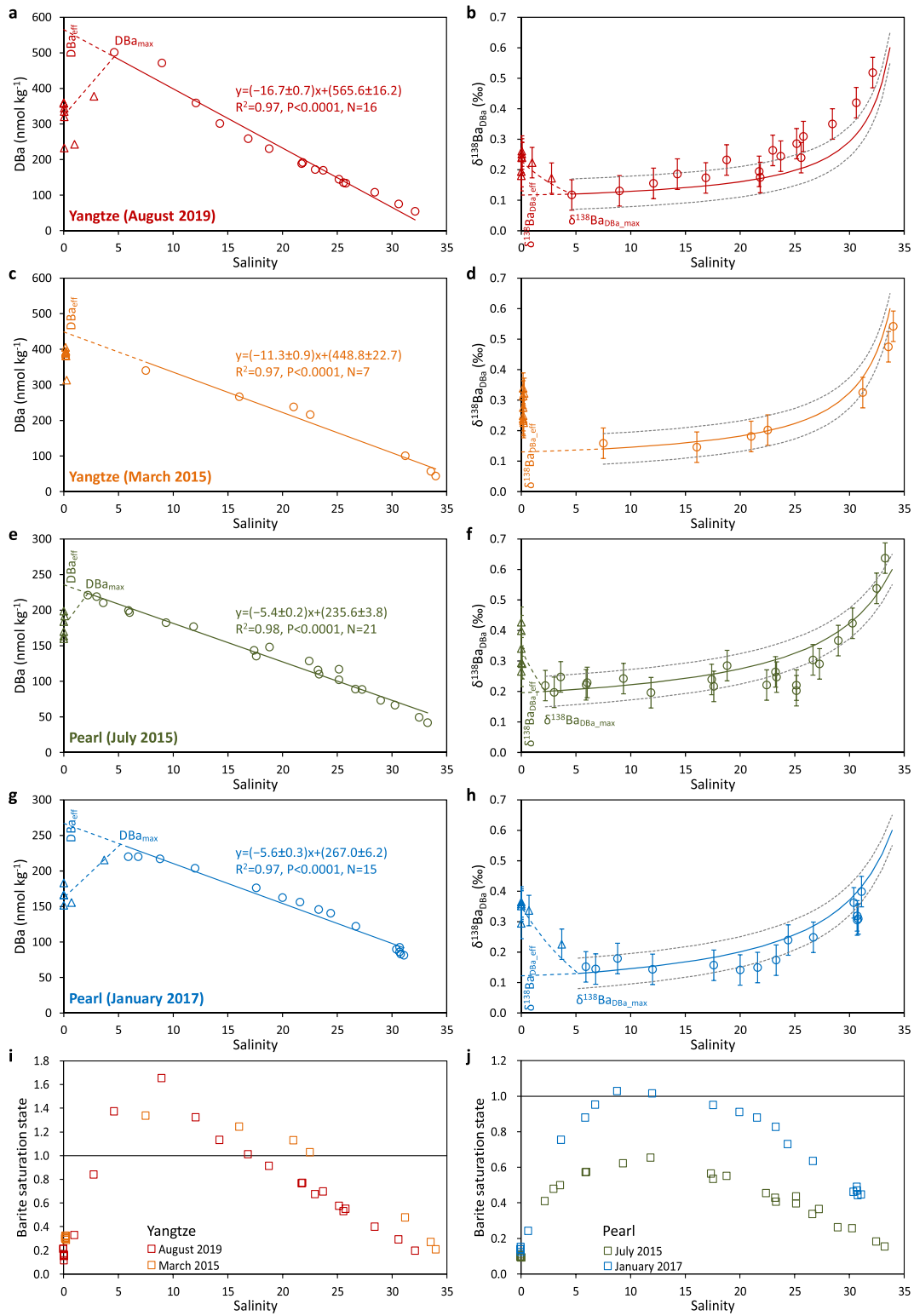


Figure 2.

In the PRE, highly significant negative DBa-salinity correlations are also observed at surface salinities  $>2.2$  in summer (July 2015;  $R^2 = 0.98$ ,  $P < 0.0001$ ,  $N = 21$ ) and  $>5.2$  in winter (January 2017;  $R^2 = 0.97$ ,  $P < 0.0001$ ,  $N = 15$ ) indicating conservative estuarine mixing beyond a  $\text{DBa}_{\text{max}}$  of 220 and 235  $\text{nmol kg}^{-1}$ , respectively.  $\text{DBa}_{\text{eff}}$  concentrations at zero salinity, estimated at 235 and 265  $\text{nmol kg}^{-1}$ , are also markedly higher than the corresponding  $\text{DBa}_{\text{sal} = 0}$ . Unlike the YRE, however, the PRE shows only minor seasonal variation in DBa distributions as well as comparable linear regression patterns beyond low salinities and in both  $\text{DBa}_{\text{max}}$  and  $\text{DBa}_{\text{eff}}$  values (Figures 2e and 2g). Nevertheless, both river estuaries are characterized by conservative two-endmember mixing of DBa concentrations between low-salinity waters at  $\text{DBa}_{\text{max}}$  and seawater.

### 3.2. Surface $\delta^{138}\text{Ba}_{\text{DBa}}$ Distributions

Based on the observed distributions of DBa concentrations we predict conservative mixing of dissolved Ba isotopes using the seawater endmember in the offshore East and South China Sea (low DBa and heavy  $\delta^{138}\text{Ba}_{\text{DBa}}$ ; Cao, Siebert, et al., 2020) and the low-salinity water endmember (high  $\text{DBa}_{\text{max}}$  and light  $\delta^{138}\text{Ba}_{\text{DBa}_{\text{max}}}$ ; Supporting Information S1). Overall, field  $\delta^{138}\text{Ba}_{\text{DBa}}$  data collected beyond  $\text{DBa}_{\text{max}}$  in both the YRE (above a salinity of 7.5 in spring) and PRE are consistent with conservative mixing predictions (Figures 2b, 2d, 2f, and 2h), suggesting that two-endmember mixing alone explains both elemental and isotopic behavior of Ba beyond low salinities. This feature has also been observed in the Amazon, Fly, and Johor River Estuary (Bridgestock et al., 2021).

The effective Ba isotopic composition of river water endmembers ( $\delta^{138}\text{Ba}_{\text{DBa}_{\text{eff}}}$ ), defined by extrapolation of the mixing-controlled  $\delta^{138}\text{Ba}_{\text{DBa}}$ -salinity relationship to zero salinity, are within error indistinguishable from the corresponding  $\delta^{138}\text{Ba}_{\text{DBa}_{\text{max}}}$  (0.1‰–0.2‰) in both the YRE and PRE. However, most field  $\delta^{138}\text{Ba}_{\text{DBa}}$  signatures at zero salinity ( $\delta^{138}\text{Ba}_{\text{DBa}_{\text{sal} = 0}}$ ; up to 0.3‰–0.4‰) in both estuaries are markedly heavier than the estimated  $\delta^{138}\text{Ba}_{\text{DBa}_{\text{eff}}}$  (Figures 2b, 2d, 2f, and 2h), implying fractionation of Ba isotopes in river waters.

The contrasting behavior of Ba isotopes below and above  $\text{DBa}_{\text{max}}$  is also indicated by the  $\delta^{138}\text{Ba}_{\text{DBa}}-1/\text{DBa}$  plots (Figure S2). A highly significant positive linear relationship is observed in both the YRE ( $R^2 = 0.94$  and  $0.99$ ,  $P < 0.0001$  and  $< 0.0001$ ,  $N = 16$  and  $7$ , in August 2019 and March 2015, respectively) and PRE ( $R^2 = 0.89$  and  $0.89$ ,  $P < 0.0001$  and  $< 0.0001$ ,  $N = 21$  and  $15$ , in July 2015 and January 2017, respectively) for data collected beyond low salinities. This confirms the two-endmember mixing of highly fractionated seawater and low-salinity water with lightest  $\delta^{138}\text{Ba}_{\text{DBa}}$  signatures. In contrast, most data points from samples close to zero salinity clearly plot above the linear regression in both estuaries (Figure S2), pointing to the role of other processes controlling the Ba isotopic signature of inputs from the drainage basin.

We, therefore, measured the  $\delta^{138}\text{Ba}_{\text{DBa}}$  of upstream freshwater samples of the Yangtze and Pearl River. While  $\delta^{138}\text{Ba}_{\text{DBa}}$  varies over a range of 0.1‰–0.3‰ during all four seasons in the Yangtze River,  $\delta^{138}\text{Ba}_{\text{DBa}}$  of  $-0.1\%$  to 0.2‰ is slightly lower in winter and spring in the Pearl River (Table S2). These  $\delta^{138}\text{Ba}_{\text{DBa}}$  signatures are overall lighter than  $\delta^{138}\text{Ba}_{\text{DBa}_{\text{sal} = 0}}$  determined in both estuaries, indicating modification of the original Ba isotopic composition of upstream freshwater during discharge into these estuaries.

### 3.3. Control of Particle Adsorption-Desorption

We suggest that adsorption to suspended fluvial particles lowers DBa concentrations (Hanor & Chan, 1977; Samanta & Dalai, 2016) and raises  $\delta^{138}\text{Ba}_{\text{DBa}}$  signatures of the river endmember in the estuaries (Bridgestock

**Figure 2.** Distributions of surface DBa,  $\delta^{138}\text{Ba}_{\text{DBa}}$ , and barite saturation state along the estuarine salinity gradient. (a and b) Yangtze River Estuary (YRE) in August 2019; (c and d) in March 2015; (e and f) Pearl River Estuary in July 2015; (g and h) in January 2017. In (a, c, e, and g), the solid lines and equations indicate the linear DBa-salinity regression fitted to the data points denoted by circles. Their extrapolation to zero salinity yields the effective DBa concentration ( $\text{DBa}_{\text{eff}}$ ) of riverine inputs to the ocean. The intersect of dashed lines predicts the DBa maximum concentration ( $\text{DBa}_{\text{max}}$ ) at low salinities, which was not calculated for the YRE in spring due to absent data. In (b, d, f, and h), the solid color lines predict the two-endmember mixing for  $\delta^{138}\text{Ba}_{\text{DBa}}$  between the low-salinity water at  $\text{DBa}_{\text{max}}$  (or the water mass at a salinity of 7.5 in the YRE in spring) and seawater; their extrapolation to zero salinity predicts the effective riverine DBa isotopic composition ( $\delta^{138}\text{Ba}_{\text{DBa}_{\text{eff}}}$ ). Dashed gray lines above and below indicate the error margin deduced from the uncertainty in estimating endmember values, which corresponds to a long-term external reproducibility for Ba isotope analyses of 0.05‰. The intersect of dashed color lines predicts the isotopic composition of  $\text{DBa}_{\text{max}}$  ( $\delta^{138}\text{Ba}_{\text{DBa}_{\text{max}}}$ ) at low salinities, which was not calculated for the YRE in spring due to absent data. In (i and j), the solid lines indicate barite saturation state = 1.

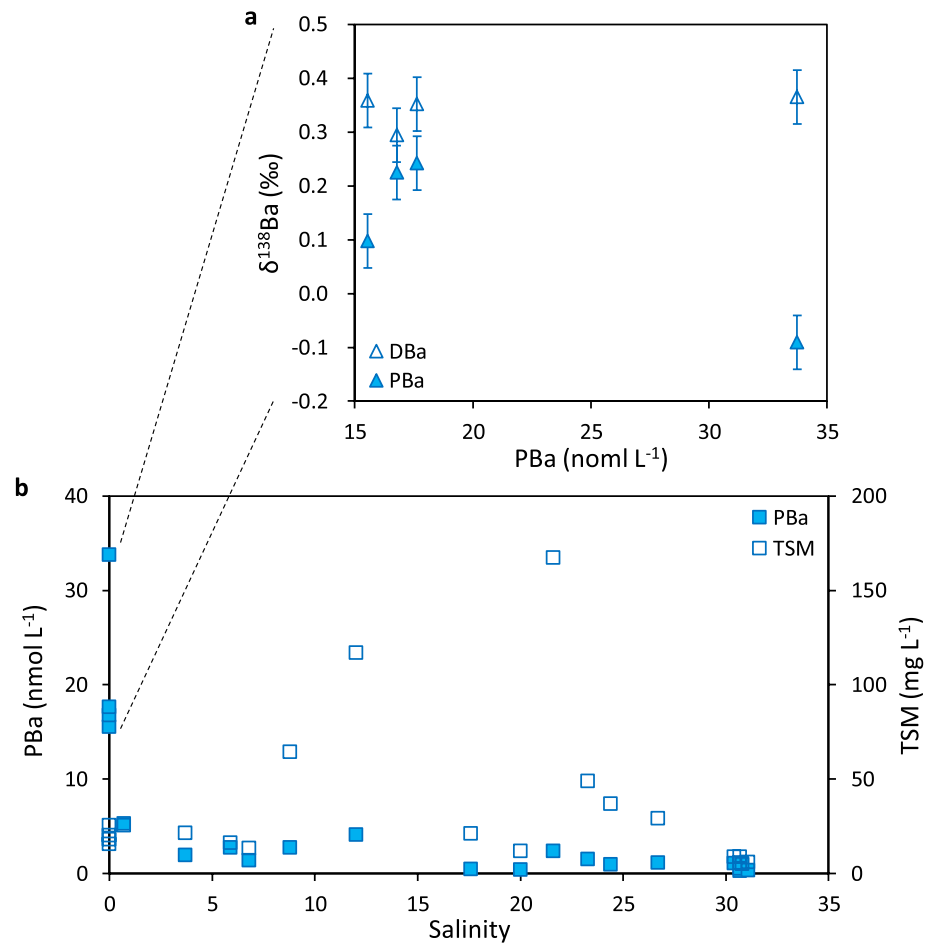


**Figure 3.** Distributions of surface exchangeable PBa and  $\delta^{138}\text{Ba}_{\text{PBa}}$  in the Pearl River Estuary in January 2017. (a)  $\delta^{138}\text{Ba}_{\text{PBa}}$  versus  $\delta^{138}\text{Ba}_{\text{DBa}}$  in the river endmember; (b) Exchangeable PBa and total suspended matter (TSM) distributions along the salinity gradient.

et al., 2021; Gou et al., 2020). This DBa removal is unlikely to result from barite precipitation due to undersaturation (i.e., barite saturation state  $<1$ ) at zero salinity in both the YRE and PRE (Figures 2i and 2j; Table S1). Using the deduced  $\text{DBa}_{\text{eff}}$  and  $\delta^{138}\text{Ba}_{\text{DBa,eff}}$  as initial values and applying the field  $\text{DBa}_{\text{sal}=0}$  and  $\delta^{138}\text{Ba}_{\text{DBa,sal}=0}$  in both Rayleigh and steady-state fractionation models (Supporting Information S1), the estimated fractionation factor of Ba isotopes ( $^{138}\epsilon$ ) during particle adsorption averages  $-0.23 \pm 0.06$  (August 2019) and  $-0.77 \pm 0.20\text{‰}$  (March 2015) in the YRE and  $-0.45 \pm 0.10$  (July 2015) and  $-0.52 \pm 0.07\text{‰}$  (January 2017) in the PRE (Table S3). Values of  $^{138}\epsilon$  for the YRE vary seasonally. The higher value obtained in spring is mainly a consequence of the lower  $\text{DBa}_{\text{eff}}$  estimate, which may be compromised by the lack of data for surface waters at salinities of 0–7.5 (Figure 2c). The lower value obtained in summer agrees well with the estimated isotope fractionation during the adsorption of Ba to particles in the Amazon, Fly, and Johor River Estuary (Bridgestock et al., 2021).

This adsorptive fractionation process in estuaries is supported by the light Ba isotopic composition (0.1‰ on average) of exchangeable particulate phases in surface water suspended particles (Table S4) collected in the PRE river endmember in January 2017 (Figure 3a). As a first-order estimate, the apparent fractionation factor  $\Delta^{138}\text{Ba}$ , given by “ $\delta^{138}\text{Ba}_{\text{PBa}} - \delta^{138}\text{Ba}_{\text{DBa}}$ ,” varies between  $-0.5\text{‰}$  and  $-0.1\text{‰}$  and is within error comparable to or slightly smaller than the  $^{138}\epsilon$  reported above.

In addition to river systems such as the middle Yellow River (Gou et al., 2020), adsorption-induced enrichment of lighter Ba isotopes in the particulate phase has also been observed in soils (Gong et al., 2019) and in seawater (Cao et al., 2016; Cao, Li, et al., 2020). In the latter case,  $^{138}\epsilon$  values of  $-0.4\text{‰}$  to  $-0.5\text{‰}$ , consistent

with those for the PRE, were obtained in the euphotic zone of the offshore South China Sea. However, van Zuilen, Müller, et al. (2016) showed an opposite direction of Ba isotope fractionation with heavier Ba isotopes being preferentially adsorbed to the surface of silica hydrogel ( $\Delta^{138}\text{Ba}_{\text{gel-solution}} \sim +0.1\text{‰}$  to  $+0.3\text{‰}$ ). This contrasting behavior may result from the difference in mineral structure between particles in natural environments and silica hydrogel under laboratory conditions (Gong et al., 2019; Gou et al., 2020). The exact mechanisms by which Ba is isotopically fractionated during particle adsorption are, however, currently unknown and need future investigations.

Another possible explanation for elevated  $\delta^{138}\text{Ba}_{\text{DBa}_{\text{sal}=0}}$  is the addition of DBa from other water masses with a distinctly heavier Ba isotope composition. Previous studies have shown that benthic inputs from either groundwater discharge or sediments play a role in estuarine Ba dynamics (Colbert & McManus, 2005; Hong et al., 2018; Joung & Shiller, 2014; Mayfield et al., 2021; Moore, 1997). Given that this influence usually decreases with increasing distance from the seafloor, we further compared dissolved Ba distributions in PRE bottom and surface waters in January 2017. Along the entire salinity gradient, data points of both bottom water DBa concentrations and  $\delta^{138}\text{Ba}_{\text{DBa}}$  signatures plot exactly on the trends defined by surface water samples (Figures S3a and S3b). For each station, bottom water DBa concentrations are comparable to or even lower than corresponding surface values, while most  $\delta^{138}\text{Ba}_{\text{DBa}}$  signatures do not differ between the two layers (Figures S3c and S3d). This essentially rules out significant benthic influence on Ba dynamics in the PRE water column.

Note that the PRE is located in one of the most rapidly developing areas of the world and has been altered significantly by anthropogenic perturbations during the past three decades. We thus measured  $\delta^{138}\text{Ba}_{\text{DBa}}$  in samples of waste waters originating from industry, agriculture, and sanitary sewage in the upper estuary in May 2016 (Table S5). The  $\delta^{138}\text{Ba}_{\text{DBa}}$  signatures vary from  $-0.1\text{‰}$  to  $0.1\text{‰}$  in the waste waters, which are too light to account for the heavy  $\delta^{138}\text{Ba}_{\text{DBa}_{\text{sal}=0}}$  observed in the PRE.

DBa concentrations in the YRE vary within a range close to that observed nearly 40 years ago (Figures 2a, 2c, and S1; Edmond et al., 1985). The newly observed distribution pattern of DBa concentrations along the entire salinity gradient in both the YRE and PRE, which does not show any pronounced enrichments, is typical of that for the majority of previously investigated estuaries including relatively pristine ones such as the Amazon and Fly River Estuary (Bridgestock et al., 2021, and references therein). These lines of evidence further support insignificant influences of human activities on estuarine Ba dynamics in our study.

Beyond the river endmember in both the YRE and PRE,  $\delta^{138}\text{Ba}_{\text{DBa}}$  signatures show a rapid decline to the lightest  $\delta^{138}\text{Ba}_{\text{DBa}_{\text{max}}}$ , which we infer results from Ba desorption from suspended fluvial particles, thereby returning isotopically light Ba to the dissolved pool (Bridgestock et al., 2021). Elevated DBa concentrations corresponding to barite saturation states above 1 at intermediate salinities (Figures 2i and 2j; Table S1) essentially exclude any significant Ba removal through barite precipitation. In the PRE in January 2017, exchangeable PBa concentrations also rapidly decrease from zero salinity ( $15\text{--}35 \text{ nmol L}^{-1}$ ) to low salinities around 5 ( $1\text{--}5 \text{ nmol L}^{-1}$ ) and remain close to zero between a salinity of 5 and the open ocean endmember. In contrast, total suspended matter concentrations are markedly lower in the river endmember ( $<25 \text{ mg L}^{-1}$ ) than at intermediate salinities of 12–22 (the highest value approaches  $170 \text{ mg L}^{-1}$ ) (Figure 3b). Consequently, particle desorption must rapidly release most of the exchangeable Ba leading to the occurrence of the highest  $\text{DBa}_{\text{max}}$  and lightest  $\delta^{138}\text{Ba}_{\text{DBa}_{\text{max}}}$  at low salinities (Coffey et al., 1997; Joung & Shiller, 2014), beyond which this process only plays a minor role in estuarine Ba dynamics.

### 3.4. Model Simulation

Considering Ba addition via salinity-induced particle desorption, we use an ion exchange model (Hanor & Chan, 1977) to simulate surface DBa and  $\delta^{138}\text{Ba}_{\text{DBa}}$  distributions, which overall agree well with field measurements in both the YRE and PRE (Figure 4). The model-derived exchangeable PBa concentrations are  $220 \pm 40$  and  $120 \pm 40 \text{ nmol L}^{-1}$  for the YRE in August 2019 and for the PRE in January 2017, respectively. Both values are consistent with estimates of DBa removal via particle adsorption in the river endmember, which approximate the difference between  $\text{DBa}_{\text{eff}}$  and  $\text{DBa}_{\text{sal}=0}$  and are 240 and  $100 \text{ nmol kg}^{-1}$  in the two cases, respectively.

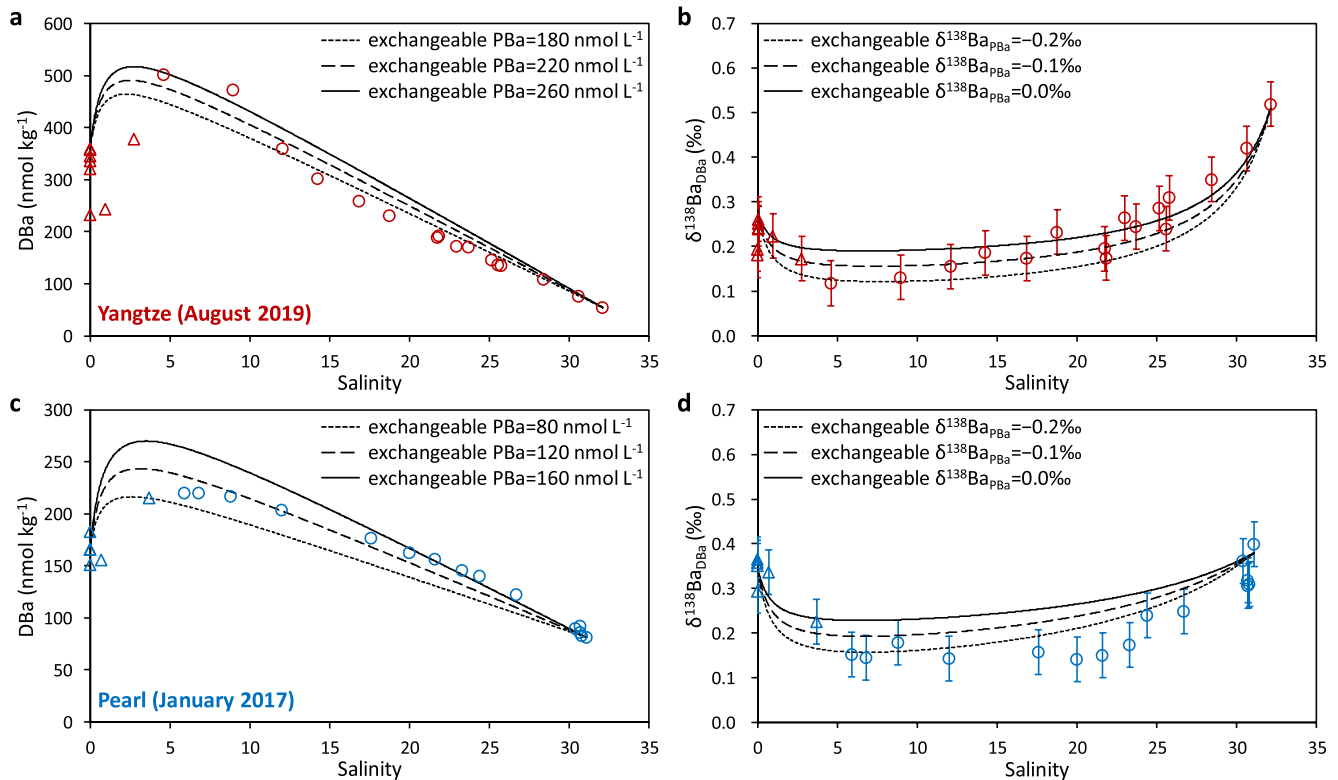


**Figure 4.** Ion exchange model results (lines) versus field measurements (symbols) of surface DBa and  $\delta^{138}\text{Ba}_{\text{DBa}}$  along the estuarine salinity gradient. (a and b) Yangtze River Estuary in August 2019; (c and d) Pearl River Estuary in January 2017. DBa simulations test changing exchangeable PBa concentrations;  $\delta^{138}\text{Ba}_{\text{DBa}}$  simulations test changing exchangeable  $\delta^{138}\text{Ba}_{\text{PBa}}$  signatures at an optimized PBa concentration (220 and 120  $\text{nmol L}^{-1}$  for the two cases, respectively). In each panel, triangles and circles denote data collected before and beyond the DBa maximum concentration estimated based on field observations, respectively.

Moreover, the model clearly generates the  $\text{DBa}_{\text{max}}$  and  $\delta^{138}\text{Ba}_{\text{DBa}_{\text{max}}}$  signals despite the fact that the corresponding salinity values appear slightly lower than our estimates based on discrete sampling (Figure 4). The model predicts a theoretical exchangeable  $\delta^{138}\text{Ba}_{\text{PBa}}$  signature of suspended fluvial particles close to  $-0.1\text{‰}$ , which is within error comparable to observations in the Yellow River drainage basin (Gou et al., 2020) and in the PRE river endmember. This value also points to an apparent  $\Delta^{138}\text{Ba}$  of  $-0.3\text{‰}$  to  $-0.5\text{‰}$  comparable to the  $^{138}\epsilon$  deduced from the fractionation models (Table S3). A few field values deviate from model results, including relatively low DBa concentrations at salinities of 14.3 and 25.8 in the YRE in August 2019 and light  $\delta^{138}\text{Ba}_{\text{DBa}}$  signatures at salinities of 20–23.3 in the PRE in January 2017 (Figures 4a and 4d). We contend that the model is an oversimplification given that assumptions such as an instantaneous equilibrium of ion exchange is unlikely realistic (Hanor & Chan, 1977). More importantly, the influence of particle adsorption-desorption substantially decreases beyond  $\text{DBa}_{\text{max}}$  in river estuaries where conservative two-endmember mixing primarily controls both elemental and isotopic behavior of dissolved Ba.

#### 4. Concluding Remarks

$\text{DBa}_{\text{eff}}$  has been adopted as a more realistic endmember than measured Ba concentrations of river waters to calculate the riverine flux of Ba to the ocean (Guay & Falkner, 1998; Shaw et al., 1998). Similarly, our findings of lighter  $\delta^{138}\text{Ba}_{\text{DBa}_{\text{eff}}}$  than  $\delta^{138}\text{Ba}_{\text{DBa}_{\text{sal}=0}}$  in two of the world's largest river estuaries emphasize the importance of solution-particle interactions in modifying the Ba properties of river water endmember, the largest source term of the global oceanic Ba budget (Carter et al., 2020). Employing the decreased  $\delta^{138}\text{Ba}_{\text{DBa}_{\text{eff}}}$  value brings the global oceanic Ba isotope mass balance closer to a steady state (Bridgestock et al., 2021), given that hydrothermal inputs contribute Ba with extremely heavy  $\delta^{138}\text{Ba}$  ( $1.7 \pm 0.7\text{‰}$ ) to the ocean (Hsieh et al., 2021).

The apparently conservative behavior of Ba isotopes beyond  $DBa_{\max}$  in both the YRE and PRE provides a prerequisite for using them as a proxy for paleosalinity, potentially opening a new avenue for quantitative reconstruction of changes in land precipitation and monsoon intensity. Combining the linear regression of  $\delta^{138}Ba_{DBa} - 1/DBa$  (Figure S2) and  $DBa$ -salinity (Figure 2) in the two estuaries, a general salinity calibration based on  $\delta^{138}Ba$  is achieved, as follows:

$$\text{Salinity} = \frac{s_1}{s_2} \times \frac{1}{\delta^{138}Ba - i_1} - \frac{i_2}{s_2} \quad (1)$$

where  $s_1$  and  $s_2$  are the slope values, and  $i_1$  and  $i_2$  are the intercept values of the two linear regressions. Note that the values obtained in this study are season- and/or site-specific (Figures 2 and S2), indicating that a globally valid calibration is not possible. However, if recorded by carbonate archives with high-temporal resolution such as coastal corals (Lewis et al., 2018; Liu et al., 2019; Tanzil et al., 2019), these specific conservative salinity- $\delta^{138}Ba_{DBa}$  relationships can serve as a basis for the realistic reconstruction of short-term and regional weather and climate events. The development of a reliable Ba isotope proxy for paleosalinity requires systematic future investigations of  $\delta^{138}Ba$  signatures of living calcifiers in the water column and their carbonate skeletons either deposited in the marine and estuarine sediments or forming coral reefs near large estuaries.

### Data Availability Statement

The dataset has been published at Science Data Bank as: Xinting Rao, Zhimian Cao. A dataset of stable barium isotopes in the Yangtze and Pearl River Estuary, China. V1. Science Data Bank. You can reach it via: <http://www.doi.org/10.11922/sciencedb.01133>. Constructive comments by two anonymous reviewers significantly improved the quality of this contribution.

### Acknowledgments

This study was funded by the National Natural Science Foundation of China (NSFC; 42022044 and 91858107). Sample collection in the Yangtze River Estuary in March 2015 and August 2019 were conducted onboard the R/V *Runjiang I* supported by a Shiptime Sharing Project of the NSFC (NORC2015-03) and the R/V *Zheyuke II* supported by the Open Cruise “KECES-2019” organized by Tongji University, respectively. Bo Liu acknowledges additional funding from the Helmholtz Association (Alfred Wegener Institute Helmholtz Centre for Polar and Marine Research). We thank Pinghe Cai, Xianghui Guo, and Weidong Zhai for their assistance in sampling and/or analyses.

### References

- Bates, S. L., Hendry, K. R., Pryer, H. V., Kinsley, C. W., Pyle, K. M., Woodward, E. M. S., & Horner, T. J. (2017). Barium isotopes reveal role of ocean circulation on barium cycling in the Atlantic. *Geochimica et Cosmochimica Acta*, 204, 286–299. <https://doi.org/10.1016/j.gca.2017.01.043>
- Bridgestock, L., Hsieh, Y.-T., Porcelli, D., Homoky, W. B., Bryan, A., & Henderson, G. M. (2018). Controls on the barium isotope compositions of marine sediments. *Earth and Planetary Science Letters*, 481, 101–110. <https://doi.org/10.1016/j.epsl.2017.10.019>
- Bridgestock, L., Nathan, J., Paver, R., Hsieh, Y.-T., Porcelli, D., Tanzil, J., et al. (2021). Estuarine processes modify the isotope composition of dissolved riverine barium fluxes to the ocean. *Chemical Geology*, 579, 120340. <https://doi.org/10.1016/j.chemgeo.2021.120340>
- Cao, Z., Li, Y., Rao, X., Yu, Y., Hathorne, E. C., Siebert, C., et al. (2020). Constraining barium isotope fractionation in the upper water column of the South China Sea. *Geochimica et Cosmochimica Acta*, 288, 120–137. <https://doi.org/10.1016/j.gca.2020.08.008>
- Cao, Z., Siebert, C., Hathorne, E. C., Dai, M., & Frank, M. (2016). Constraining the oceanic barium cycle with stable barium isotopes. *Earth and Planetary Science Letters*, 434, 1–9. <https://doi.org/10.1016/j.epsl.2015.11.017>
- Cao, Z., Siebert, C., Hathorne, E. C., Dai, M., & Frank, M. (2020). Corrigendum to “Constraining the oceanic barium cycle with stable barium isotopes”. *Earth and Planetary Science Letters*, 434, 1–9.
- Carter, S. C., Paytan, A., & Griffith, E. M. (2020). Toward an improved understanding of the marine barium cycle and the application of marine barite as a paleoproductivity proxy. *Minerals*, 10, 421. <https://doi.org/10.3390/min10050421>
- Coffey, M., Dehairs, F., Collette, O., Luther, G., Church, T., & Jickells, T. (1997). The behaviour of dissolved barium in estuaries. *Estuarine, Coastal and Shelf Science*, 45, 113–121. <https://doi.org/10.1006/ecss.1996.0157>
- Colbert, D., & McManus, J. (2005). Importance of seasonal variability and coastal processes on estuarine manganese and barium cycling in a Pacific Northwest estuary. *Continental Shelf Research*, 25, 1395–1414. <https://doi.org/10.1016/j.csr.2005.02.003>
- Edmond, J. M., Spivack, A., Grant, B. C., Hu, M.-H., Chen, Z., Chen, S., & Zeng, X. (1985). Chemical dynamics of the Changjiang estuary. *Continental Shelf Research*, 4, 17–36. [https://doi.org/10.1016/0278-4343\(85\)90019-6](https://doi.org/10.1016/0278-4343(85)90019-6)
- Gebregiorgis, D., Hathorne, E. C., Sijinkumar, A. V., Nath, B. N., Nürnberg, D., & Frank, M. (2016). South Asian Summer Monsoon variability during the last ~54kyrs inferred from surface water salinity and river run off proxies. *Quaternary Science Reviews*, 138, 6–15. <https://doi.org/10.1016/j.quascirev.2016.02.012>
- Geyman, B. M., Ptacek, J. L., LaVigne, M., & Horner, T. J. (2019). Barium in deep-sea bamboo corals: Phase associations, barium stable isotopes, and prospects for paleoceanography. *Earth and Planetary Science Letters*, 525, 115751. <https://doi.org/10.1016/j.epsl.2019.115751>
- Gong, Y., Zeng, Z., Zhou, C., Nan, X., Yu, H., Lu, Y., et al. (2019). Barium isotopic fractionation in latosol developed from strongly weathered basalt. *The Science of the Total Environment*, 687, 1295–1304. <https://doi.org/10.1016/j.scitotenv.2019.05.427>
- Gou, L.-F., Jin, Z., Galy, A., Gong, Y.-Z., Nan, X.-Y., Jin, C., et al. (2020). Seasonal riverine barium isotopic variation in the middle Yellow River: Sources and fractionation. *Earth and Planetary Science Letters*, 531, 115990. <https://doi.org/10.1016/j.epsl.2019.115990>
- Guay, C. K., & Falkner, K. K. (1997). Barium as a tracer of Arctic halocline and river waters. *Deep-Sea Research Part II*, 44, 1543–1569. [https://doi.org/10.1016/S0967-0645\(97\)00066-0](https://doi.org/10.1016/S0967-0645(97)00066-0)
- Guay, C. K., & Falkner, K. K. (1998). A survey of dissolved barium in the estuaries of major Arctic rivers and adjacent seas. *Continental Shelf Research*, 18, 859–882. [https://doi.org/10.1016/S0278-4343\(98\)00023-5](https://doi.org/10.1016/S0278-4343(98)00023-5)

- Hanor, J. S., & Chan, L.-H. (1977). Non-conservative behavior of barium during mixing of Mississippi River and Gulf of Mexico waters. *Earth and Planetary Science Letters*, 37, 242–250. [https://doi.org/10.1016/0012-821x\(77\)90169-8](https://doi.org/10.1016/0012-821x(77)90169-8)
- Hemsing, F., Hsieh, Y.-T., Bridgestock, L., Spooner, P. T., Robinson, L. F., Frank, N., & Henderson, G. M. (2018). Barium isotopes in cold-water corals. *Earth and Planetary Science Letters*, 491, 183–192. <https://doi.org/10.1016/j.epsl.2018.03.040>
- Hong, Q., Cai, P., Geibert, W., Cao, Z., Stimac, I., Liu, L., & Li, Q. (2018). Benthic fluxes of metals into the Pearl River Estuary based on  $^{224}\text{Ra}/^{228}\text{Th}$  disequilibrium: From alkaline earth elements (Ba) to redox sensitive metals (U, Mn, and Fe). *Geochimica et Cosmochimica Acta*, 237, 223–239. <https://doi.org/10.1016/j.gca.2018.06.036>
- Horner, T. J., Kinsley, C. W., & Nielsen, S. G. (2015). Barium-isotopic fractionation in seawater mediated by barite cycling and ocean circulation. *Earth and Planetary Science Letters*, 430, 511–522. <https://doi.org/10.1016/j.epsl.2015.07.027>
- Hsieh, Y.-T., Bridgestock, L., Scheuermann, P. P., Seyfried, W. E., Jr., & Henderson, G. M. (2021). Barium isotopes in mid-ocean ridge hydrothermal vent fluids: A source of isotopically heavy Ba to the ocean. *Geochimica et Cosmochimica Acta*, 292, 348–363. <https://doi.org/10.1016/j.gca.2020.09.037>
- Hsieh, Y.-T., & Henderson, G. M. (2017). Barium stable isotopes in the global ocean: Tracer of Ba inputs and utilization. *Earth and Planetary Science Letters*, 473, 269–278. <https://doi.org/10.1016/j.epsl.2017.06.024>
- Joung, D., & Shiller, A. M. (2014). Dissolved barium behavior in Louisiana Shelf waters affected by the Mississippi/Atchafalaya River mixing zone. *Geochimica et Cosmochimica Acta*, 141, 303–313. <https://doi.org/10.1016/j.gca.2014.06.021>
- Lewis, S. E., Lough, J. M., Cantin, N. E., Matson, E. G., Kinsley, L., Bainbridge, Z. T., & Brodie, J. E. (2018). A critical evaluation of coral Ba/Ca, Mn/Ca and Y/Ca ratios as indicators of terrestrial input: New data from the Great Barrier Reef, Australia. *Geochimica et Cosmochimica Acta*, 237, 131–154. <https://doi.org/10.1016/j.gca.2018.06.017>
- Liu, Y., Li, X., Zeng, Z., Yu, H.-M., Huang, F., Felis, T., & Shen, C.-C. (2019). Annually-resolved coral skeletal  $\delta^{138/134}\text{Ba}$  records: A new proxy for oceanic Ba cycling. *Geochimica et Cosmochimica Acta*, 247, 27–39. <https://doi.org/10.1016/j.gca.2018.12.022>
- Mayfield, K. K., Eisenhauer, A., Santiago Ramos, D. P., Higgins, J. A., Horner, T. J., Auro, M., et al. (2021). Groundwater discharge impacts marine isotope budgets of Li, Mg, Ca, Sr, and Ba. *Nature Communications*, 12, 148. <https://doi.org/10.1038/s41467-020-20248-3>
- Moore, W. S. (1997). High fluxes of radium and barium from the mouth of the Ganges-Brahmaputra River during low river discharge suggest a large groundwater source. *Earth and Planetary Science Letters*, 150, 141–150. [https://doi.org/10.1016/s0012-821x\(97\)00083-6](https://doi.org/10.1016/s0012-821x(97)00083-6)
- Preter, C., van Zuilen, K., Nägler, T. F., Reynaud, S., Böttcher, M. E., & Samankassou, E. (2016). Constraints on barium isotope fractionation during aragonite precipitation by corals. *Depositional Record*, 1, 118–129. <https://doi.org/10.1002/dep2.8>
- Samanta, S., & Dalai, T. K. (2016). Dissolved and particulate Barium in the Ganga (Hooghly) River estuary, India: Solute-particle interactions and the enhanced dissolved flux to the oceans. *Geochimica et Cosmochimica Acta*, 195, 1–28. <https://doi.org/10.1016/j.gca.2016.09.005>
- Schlitzer, R. (2021). *Ocean data view 5*. <http://odv.awi.de>
- Shaw, T. J., Moore, W. S., Kloepfer, J., & Sochaski, M. A. (1998). The flux of barium to the coastal waters of the southeastern USA: The importance of submarine groundwater discharge. *Geochimica et Cosmochimica Acta*, 62, 3047–3054. [https://doi.org/10.1016/s0016-7037\(98\)00218-x](https://doi.org/10.1016/s0016-7037(98)00218-x)
- Stecher, H. A., III, & Kogut, M. B. (1999). Rapid barium removal in the Delaware estuary. *Geochimica et Cosmochimica Acta*, 63, 1003–1012. [https://doi.org/10.1016/s0016-7037\(98\)00310-x](https://doi.org/10.1016/s0016-7037(98)00310-x)
- Tanzil, J. T. L., Goodkin, N. F., Sin, T. M., Chen, M. L., Fabbro, G. N., Boyle, E. A., et al. (2019). Multi-colony coral skeletal Ba/Ca from Singapore's turbid urban reefs: Relationship with contemporaneous in-situ seawater parameters. *Geochimica et Cosmochimica Acta*, 250, 191–208. <https://doi.org/10.1016/j.gca.2019.01.034>
- van Zuilen, K., Müller, T., Nägler, T. F., Dietzel, M., & Küsters, T. (2016). Experimental determination of barium isotope fractionation during diffusion and adsorption processes at low temperatures. *Geochimica et Cosmochimica Acta*, 186, 226–241. <https://doi.org/10.1016/j.gca.2016.04.049>
- von Allmen, K., Böttcher, M. E., Samankassou, E., & Nägler, T. F. (2010). Barium isotope fractionation in the global barium cycle: First evidence from barium minerals and precipitation experiments. *Chemical Geology*, 277, 70–77. <https://doi.org/10.1016/j.chemgeo.2010.07.011>
- Weldeab, S., Frank, M., Stichel, T., Haley, B., & Sengen, M. (2011). Spatio-temporal evolution of the West African monsoon during the last deglaciation. *Geophysical Research Letters*, 38, L13703. <https://doi.org/10.1029/2011GL047805>
- Weldeab, S., Lea, D. W., Schneider, R. R., & Andersen, N. (2007). 155,000 years of West African monsoon and ocean thermal evolution. *Science*, 316, 1303–1307. <https://doi.org/10.1126/science.1140461>
- Weldeab, S., Menke, V., & Schmiedl, G. (2014). The pace of East African monsoon evolution during the Holocene. *Geophysical Research Letters*, 41, 1724–1732. <https://doi.org/10.1002/2014GL059361>
- Yu, Y., Siebert, C., Fietzke, J., Goepfert, T., Hathorne, E. C., Cao, Z., & Frank, M. (2020). The impact of MC-ICP-MS plasma conditions on the accuracy and precision of stable isotope measurements evaluated for barium isotopes. *Chemical Geology*, 549, 119697. <https://doi.org/10.1016/j.chemgeo.2020.119697>

## References From the Supporting Information

- Cai, W.-J., Dai, M., Wang, Y., Zhai, W., Huang, T., Chen, S., et al. (2004). The biogeochemistry of inorganic carbon and nutrients in the Pearl River estuary and the adjacent Northern South China Sea. *Continental Shelf Research*, 24, 1301–1319. <https://doi.org/10.1016/j.csr.2004.04.005>
- Harrison, P. J., Yin, K., Lee, J. H. W., Gan, J., & Liu, H. (2008). Physical-biological coupling in the Pearl River Estuary. *Continental Shelf Research*, 28, 1405–1415. <https://doi.org/10.1016/j.csr.2007.02.011>
- Kang, P., Zhang, H., Zhu, Y., Liu, J., He, B., Li, Q., et al. (2021). A model of algal organic carbon distributions in the Pearl River estuary using the amino acid carbon isotope signature. *Geochimica et Cosmochimica Acta*, 294, 1–12. <https://doi.org/10.1016/j.gca.2020.11.010>
- Monnin, C. (1999). A thermodynamic model for the solubility of barite and celestite in electrolyte solutions and seawater from 0 to 200°C and to 1 kbar. *Chemical Geology*, 153, 187–209. [https://doi.org/10.1016/s0009-2541\(98\)00171-5](https://doi.org/10.1016/s0009-2541(98)00171-5)
- Patra, S., Liu, C., Wang, F., Li, S., & Wang, B. (2012). Behavior of major and minor elements in a temperate river estuary to the coastal sea. *International Journal of Environmental Science and Technology*, 9, 647–654. <https://doi.org/10.1007/s13762-012-0097-8>
- Rushdi, A. I., McManus, J., & Collier, R. W. (2000). Marine barite and celestite saturation in seawater. *Marine Chemistry*, 69, 19–31. [https://doi.org/10.1016/s0304-4203\(99\)00089-4](https://doi.org/10.1016/s0304-4203(99)00089-4)

- Siebert, C., Nägler, T. F., & Kramers, J. D. (2001). Determination of molybdenum isotope fractionation by double-spike multicollector inductively coupled plasma mass spectrometry. *Geochemistry, Geophysics, Geosystems*, 2, 1032. <https://doi.org/10.1029/2000gc000124>
- van Zuilen, K., Nägler, T. F., & Bullen, T. D. (2016). Barium isotopic compositions of geological reference materials. *Geostandards and Geoanalytical Research*, 40, 543–558. <https://doi.org/10.1111/ggr.12122>
- Wang, Y., Shen, J., He, Q., Zhu, L., & Zhang, D. (2015). Seasonal variations of transport time of freshwater exchanges between Changjiang Estuary and its adjacent regions. *Estuarine, Coastal and Shelf Science*, 157, 109–119. <https://doi.org/10.1016/j.ecss.2015.03.008>
- Zhang, A., Zhang, J., Hu, J., Zhang, R., & Zhang, G. (2015). Silicon isotopic chemistry in the Changjiang Estuary and coastal regions: Impacts of physical and biogeochemical processes on the transport of riverine dissolved silica. *Journal of Geophysical Research: Oceans*, 120, 6943–6957. <https://doi.org/10.1002/2015jc011050>
- Zhang, J., Yu, Z., Wang, J., Ren, J., Chen, H., Xiong, H., et al. (1999). The subtropical Zhujiang (Pearl River) Estuary: Nutrient, trace species and their relationship to photosynthesis. *Estuarine, Coastal and Shelf Science*, 49, 385–400. <https://doi.org/10.1006/ecss.1999.0500>